Pergamon

Available online at www.sciencedirect.com
SCIENCE DIRECT®

Cement and Concrete Research 33 (2003) 1423–1432

CEMENT AND CONCRETE RESEARCH

Microstructural investigations of naturally and artificially weathered autoclaved aerated concrete

Hülya Kus*, Thomas Carlsson

Division of Materials Technology and KTH Research School, Centre for Built Environment, University of Gävle, SE-801 76 Gävle, Sweden

Received 3 July 2002; accepted 26 February 2003

Abstract

The microstructural changes in autoclaved aerated concrete (AAC), particularly due to chemical degradation, have been investigated. The carbonation process has been studied on naturally and artificially weathered AAC by spectrographic and microscopic analysis. Visual inspections of unexposed and aged AAC were made by means of light optical microscopy and scanning electron microscopy (SEM), while chemical and structural analysis were based on X-ray diffraction (XRD) and energy-dispersive spectroscopy (EDS). The results obtained from two different experimental exposure set-ups, i.e., natural and artificial weathering, are presented. Thin-section images clearly indicate leaching out of the surface layer resulting in open larger air voids. Both naturally and artificially weathered samples displayed similar ageing characteristics in terms of mineralogical changes. The XRD patterns confirm that tobermorite were gradually transforming into calcium carbonate with exposure time. Calcite and gypsum were the two main crystal structures growing during weathering as detected in the SEM + EDS examinations.

Keywords: Autoclaved aerated concrete; Carbonation; Characterisation; Ageing; Microstructure

1. Introduction

Autoclaved aerated concrete (AAC) is manufactured by steam curing of raw materials consisting of cement, lime and gypsum as binders, fine siliceous material, pore-generating aluminium powder and water. The chemical reaction caused by addition of aluminium makes the mixture expand to about twice its volume, resulting in a highly porous structure. Approximately 80% of the volume of the hardened material is made up of pores, 50% being air pores and 30% being micropores characterised by their ability in capillary moisture transport. The microstructure of the solid matrix is mainly made up of microcrystalline platelets of tobermorite, forming the pore walls [1].

Carbonation is one of the main degradation mechanisms that possibly affects the durability and service life of concrete materials in general. Carbonation occurs when portlandite [$Ca(OH)_2$] and other calcium-bearing C-S-H phases react with CO_2 to form calcite ($CaCO_3$). Major mineralogical changes associated with carbonation include conversion of calcium silicate hydrate gel, in this case, tobermorite:

$$5CaO \cdot 6SiO_2 \cdot 5H_2O + 5CO_2 \rightarrow 5CaCO_3 + 6SiO_2 + 5H_2O \quad (1)$$

$$5CaO \cdot 6SiO_2 \cdot 5H_2O \leftrightarrow 5Ca(OH)_2 + 6SiO_2 \quad (2)$$

and portlandite:

$$Ca(OH)_2 + CO_2 \rightarrow CaCO_3 + H_2O \quad (3)$$

Degradation process is further accelerated by high concentrations of sulphur dioxide in the air. SO_2 in the presence of moisture forms sulphurous acid. By atmospheric oxygen, sulphurous acid is oxidised to sulphuric acid, which attacks calcium carbonate. Gypsum crystals occur as a reaction product.

$$SO_2 + H_2O \rightarrow H_2SO_3 \quad (4)$$

$$H_2SO_4 + CaCO_3 + H_2O \rightarrow CaSO_4 \cdot 2H_2O + CO_2 \quad (5)$$

Carbon dioxide in the presence of moisture forms carbonic acid, which reacts with $CaCO_3$, and thus produces

* Corresponding author. Faculty of Architecture, Istanbul Technical University, Taskisla, Taksim, TR-80191 Istanbul, Turkey. Tel.: +90-212-293-1300; fax: +90-212-251-4895.
E-mail address: kushu@itu.edu.tr (H. Kus).

0008-8846/03/$ – see front matter © 2003 Elsevier Ltd. All rights reserved.
doi:10.1016/S0008-8846(03)00084-X

calcium bicarbonate, which is soluble in water. As a result of calcium loss after an effective washout, erosion occurs.

$$CO_2 + H_2O \rightarrow H_2CO_3 \quad (6)$$

$$H_2CO_3 + CaCO_3 \rightarrow Ca(HCO_3)_2 \quad (7)$$

Current research mostly focuses on carbonation of concrete mainly because of the corrosion problems, whereas only some research is dealing with the carbonation of AAC. Moreover, there is only limited discussion found in the literature about the microstructural changes of AAC during natural and artificial weathering [2,3]. The aim of this study is to investigate the chemical degradation of AAC by observing and analysing the changes in the microstructure during natural and artificial weathering. The interrelation between the microstructure and the physical properties of freeze–thaw submitted, rendered AAC with different surface treatments, was studied earlier [4]. Generally, alternate wetting and drying cycles cause dissolution and reprecipitation or recrystallisation, leading to degradation of AAC as well as in other inorganic building materials [5–8]. The mechanisms involved in the deterioration of porous materials by salts are summarised through a comprehensive literature survey in an article by Charola [9].

To examine the chemical degradation in detail, the microstructure of unexposed and weathered AAC samples has been studied by means of light optical (thin section) microscopy, scanning electron microscopy (SEM), energy-dispersive spectroscopy (EDS) and X-ray diffractometry (XRD). Results obtained from two different experimental set-ups, i.e., natural and laboratory-accelerated weathering, are presented.

2. Experimental

2.1. Test samples

In the investigations carried out, lime-cement-based AAC having a dry density of 423 kg/m^3 was used. Before natural and artificial weathering, the faces of the samples were sealed with epoxy, except for the surface to be exposed. The naturally weathered samples, measuring $130 \times 130 \times 150$ mm, were exposed for 6, 18 and 36 months on a 45° rack facing south to the climate conditions of Gävle, Sweden. Gävle has a similar climate to the rest of central Sweden. According to the microclimate data monitored at the field exposure set-up during natural weathering, the yearly average air temperature in winter and in summer is −2.7 and 16.2 °C, respectively; the minimum being −22.5 °C and the maximum 29.3 °C. The ground is normally covered with snow between November and March. The average yearly total rainfall is ∼638 mm. The average SO_2 level is 2–2.5 μg/m^3, somewhat higher during cold winter days.

The artificially aged samples, measuring $65 \times 150 \times 90$ mm, were subjected to continuous exposure of light and intermittent exposure of water spray in a water-cooled xenon-arc lamp Weather-Ometer. The testing programme was operated in accordance with the test procedure described in the standard ASTM G155-00a$^{\varepsilon 1}$ [10]. Each cycle consisted of 102 min of light, followed by a cycle of 18 min of light and water spray. The artificially weathered samples were tested and analysed after 500, 1000, 1500 and 2500 h of exposure in the climate chamber. Still, there are samples being further exposed, both naturally and artificially.

2.2. Microscopy

The air-void system of unexposed and exposed AAC was characterised by thin sections having an area of approximately 20×40 mm and a thickness of approximately 25 μm impregnated with fluorescent epoxy. SEM imaging was utilised to determine detailed information on phase, chemical and textural composition and spatial distribution in the AAC microstructure. Samples taken from the unexposed and naturally and artificially weathered AAC were examined using a Hitachi S-3000 N SEM, uncoated in backscattered electron mode.

2.3. Chemical and structural analysis

Different phases formed during weathering and observed in SEM were identified in terms of chemical elements using EDS analysis performed by a Link Inca energy-dispersive X-ray system. The crystalline phases of powdered samples mainly taken from the first 1 to 2 mm of the unexposed and weathered AAC surface layers were analysed by means of a Bruker AXS D8 Advance XRD operated at 40 kV and 40 mA using CuKα radiation. The measurement range was 5–85° 2θ stepscan mode with a step size of 0.01°/1 s and a sample rotation of 60 rpm. The total measurement time amounted to about 2 h and 13 min. Investigations were based only on the qualitative assessment of collected XRD data. The minerals present in the samples were identified by matching the diffraction patterns with the standard patterns in the powder diffraction file of ICDD PDF-2 set 1–50, 70–88.

3. Results and discussion

3.1. Thin-section microscopy image analysis

The observations by thin-section microscopy of the weathered AAC samples clearly demonstrated the propagation of dissolution and the progress of carbonation from the surface to the core. The carbonation depth increased with increasing exposure time. Due to the washing out and the subsequent erosion, the air voids near the surface zone were opened. Figs. 1 and 2 illustrate the gradual leaching and the

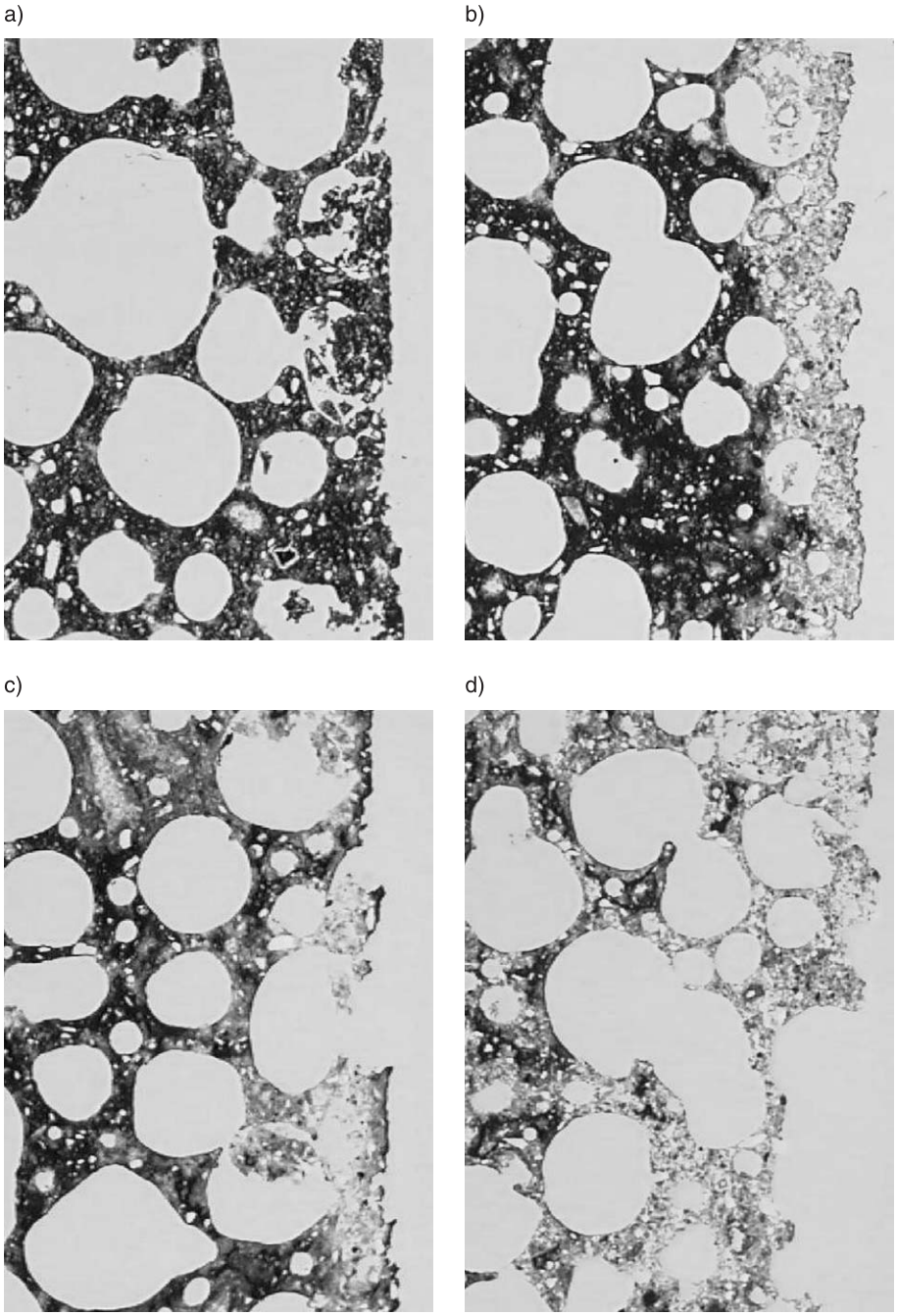

Fig. 1. The gradual leaching of surface (right of the figures): naturally aged AAC samples (image dimensions: 3.4 × 4.8 mm). (a) Unexposed; (b) 6 months; (c) 18 months; (d) 36 months.

carbonation depth of the naturally and artificially aged samples, respectively. In the pictures, the lighter parts starting from the exposed surface represent the carbonated zones, propagating inwards with time. The leaching process caused mass loss, which led to collapsed and coarsened air voids. On the other hand, some of the voids were filled up by the leachate transportation. The surface material covering the larger air voids leached out and left behind a more porous surface. The strength of the material decreased whereas the permeability increased.

3.2. SEM+EDS

The microstructural characteristics of unexposed and weathered AAC examined by SEM in backscattered mode are exemplified in the following figures. Regarding the weathered AAC samples, either naturally or artificially, EDS analyses revealed high concentration of calcium and oxygen elements in the carbonated areas and, in addition, sulphur in the gypsum crystals. Accordingly, the two main crystal growth forms in the aged AAC samples were found to

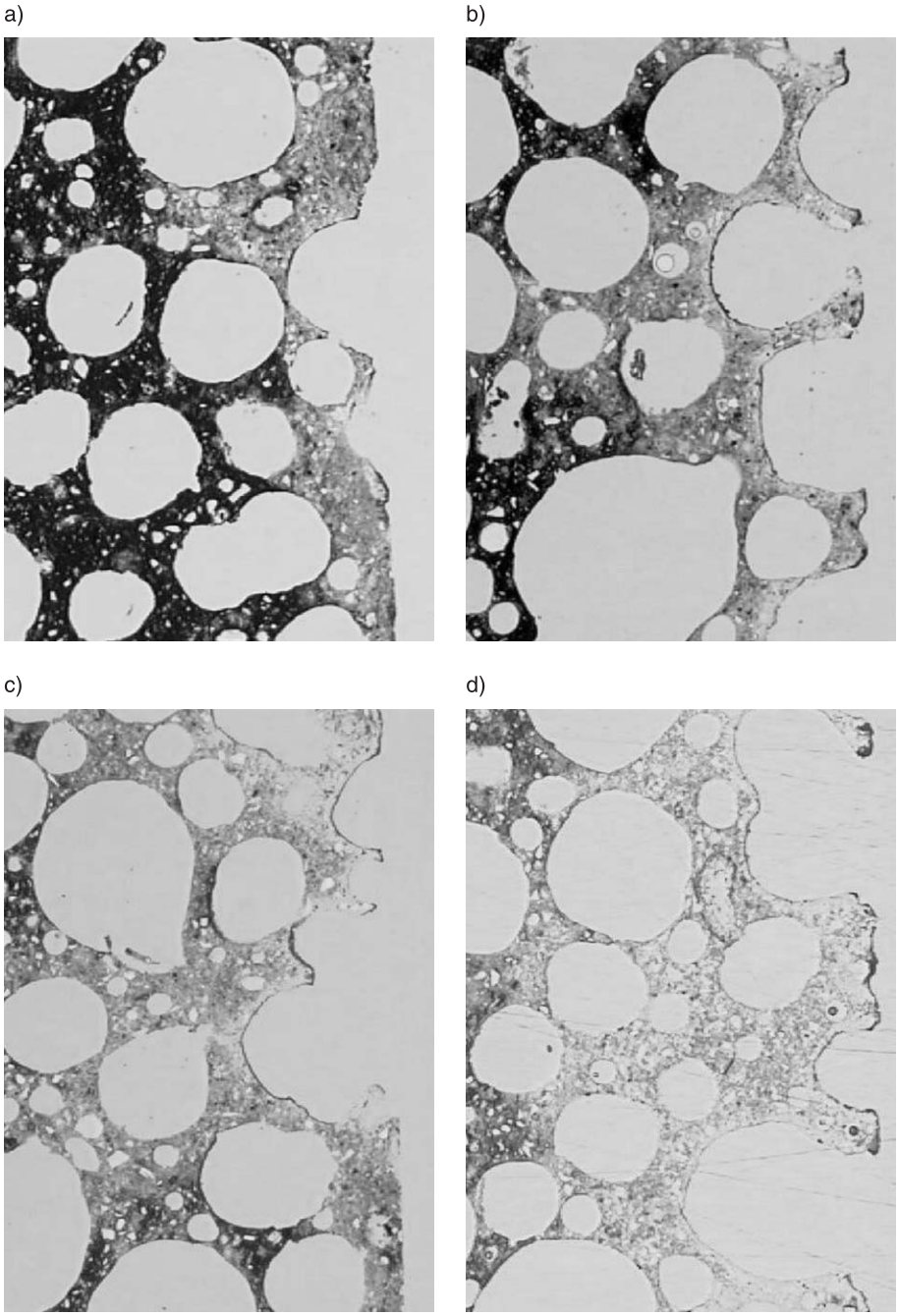

Fig. 2. The gradual leaching of surface (right of the figures): artificially weathered AAC samples (image dimensions: 3.4 × 4.8 mm). (a) 500 h; (b) 1000 h; (c) 1500 h; (d) 2500 h.

be calcite and gypsum. The presence of calcite and gypsum in the aged samples was demonstrated visually by SEM micrographs, whereas the identification of the minerals was supported by the EDS analysis of the selected targets and subsequently verified by the XRD analysis.

Fig. 3a shows a micrograph of a cross-section from the unexposed AAC surface. The air voids at the surface are covered with the microporous solid AAC matrix forming a dense surface layer, which was also illustrated by thin-section microscopy (see Fig. 1a). A micrograph from the unexposed AAC surface is shown in Fig. 3b. Evenly distributed needle-shaped gypsum single crystals were observed both in the cross-sections and on the surface. In general, the unexposed samples demonstrated nicely shaped spherical air voids (Fig. 3c) and undamaged microporous C-S-H gel in the form of tobermorite platelets (Fig. 3d). Very small calcite particles were occasionally detected in the unexposed AAC material, which can be interpreted as an

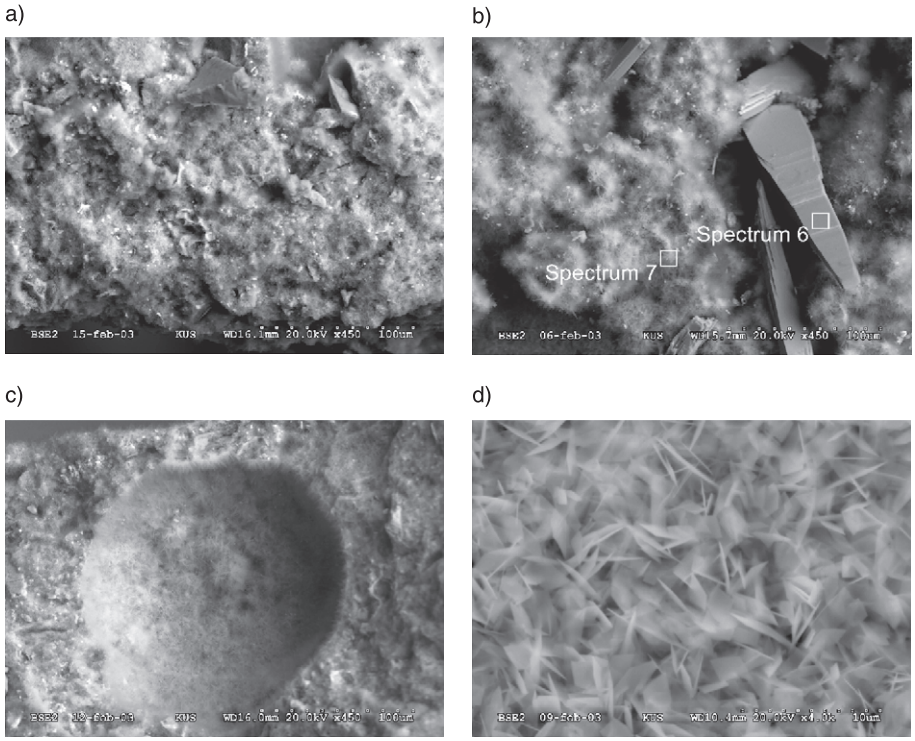

Fig. 3. SEM micrographs from the unexposed AAC sample. (a) Cross-section from the surface (bottom of the figure) (magnification: ×450); (b) Surface (magnification: ×450); (c) Air void from the cross-section (magnification: ×450); (d) Tobermorite platelets (magnification: ×4.0k).

early carbonation phase. It is important to note here that the microstructural analysis of the unexposed sample was carried out after 4 years of storage in the laboratory. However, the sample was from the same production batch as all other samples that were exposed.

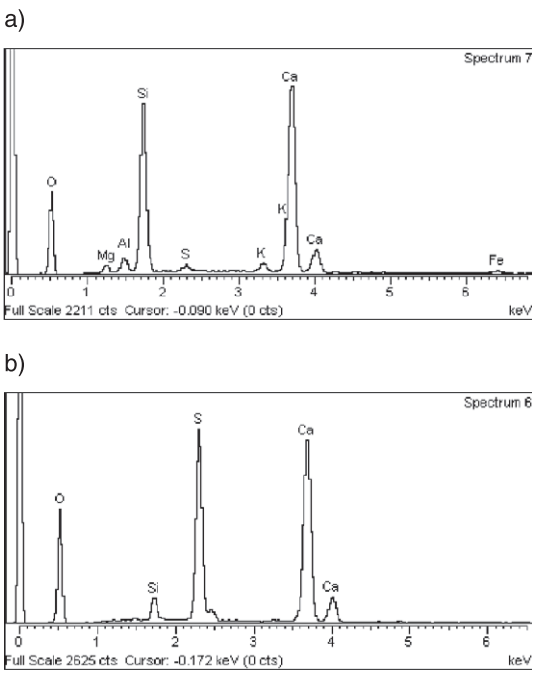

Fig. 4. EDS spectra of selected targets taken from the SEM image in Fig. 3b. (a) Spectrum 7; (b) Spectrum 6.

In Fig. 4a, the average elemental composition of the unexposed AAC sample analysed by SEM + EDS (taken from the selected target in Fig. 3b) is given as a spectral diagram. Spectrum 7 in Fig. 4a exhibits high-intensity peaks for calcium (Ca), silicon (Si) and oxygen (O), indicating the major elements that compose the C-S-H gel. Other elements comprised by the AAC material including aluminium (Al), sulphur (S), iron (Fe), etc., are also represented in the spectrum, but with rather low-intensity peaks. Fig. 4b shows the EDS spectrum of the crystal form seen in Fig. 3b. Spectrum 6, given in Fig. 4b, exhibits strong peaks for sulphur, calcium and oxygen while a weaker peak for silicon is shown, indicating that the crystal form is gypsum. Tables 1 and 2 show the EDS

Table 1
EDS raw data of Spectrum 7 in Fig. 4a

Element	Weight (%)	Atomic (%)
O	52.4	69.9
Mg	1.1	0.9
Al	1.5	1.2
Si	17.7	13.4
S	0.6	0.4
K	1.0	0.6
Ca	25.0	13.3
Fe	0.7	0.3
Total	100.0	100.0

Table 2
EDS raw data of Spectrum 6 in Fig. 4b

Element	Weight (%)	Atomic (%)
O	60.1	77.0
Si	2.1	1.6
S	15.9	10.2
Ca	21.9	11.2
Total	100.0	100.0

raw data corresponding to the spectra given in Fig. 4a and b, respectively.

Fig. 5a and b shows micrographs of cross-sections from the naturally and artificially weathered AAC surface, respectively. In the figures, the light particles (parts) indicate the decomposition of C-S-H gel into calcium carbonate in the form of calcite, i.e., carbonation. The process starts from the exposed surface and propagates inwards, the rate depending mainly on the porosity and the moisture content of the AAC material.

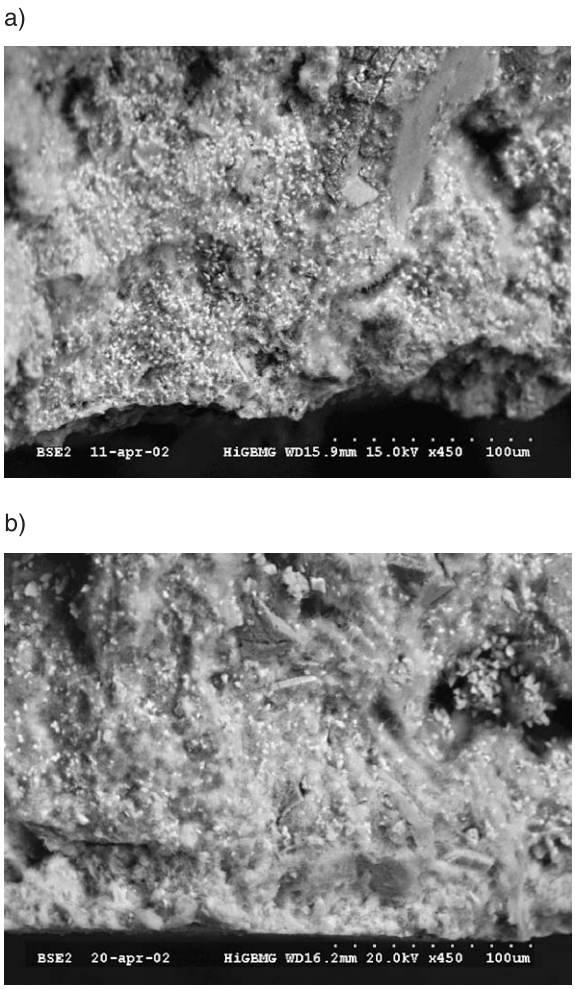

Fig. 5. SEM micrographs of cross-sections from the weathered AAC sample surfaces (bottom of the figures) showing carbonation (magnification: × 450). (a) 18 months naturally weathered; (b) 1500 h artificially weathered.

Fig. 6a and b shows images of an air void from the naturally and artificially exposed samples showing calcite precipitation throughout the samples. The corresponding electron-dispersive X-ray spectral data are given in Tables 3 and 4. EDS results indicate significantly high contents of Ca and O but rather low of Si, which was interpreted as calcite mineral after correlation with the XRD results. SEM examinations of aged samples exhibited approximately a linear increase in the content of calcite with exposure time. The concentration of calcite precipitation was observed to be highest at the surface zone and occurred mostly in the larger air voids. As can be seen in the images, the naturally and the artificially weathered samples exhibited quite good similarity in precipitation of calcite crystals in the AAC material.

During exposure, calcite crystals are coarsening to gradually form a cover on the surface (Fig. 7 and Table 5) but are also washed out and removed in the longer term. This type of calcite layer formation was only observed on the 1500-h artificially exposed sample surface. The calcite particles on the naturally exposed surface appeared no longer in the sharp crystal form observed inside the material but were interfusing with gypsum. This is probably because of the

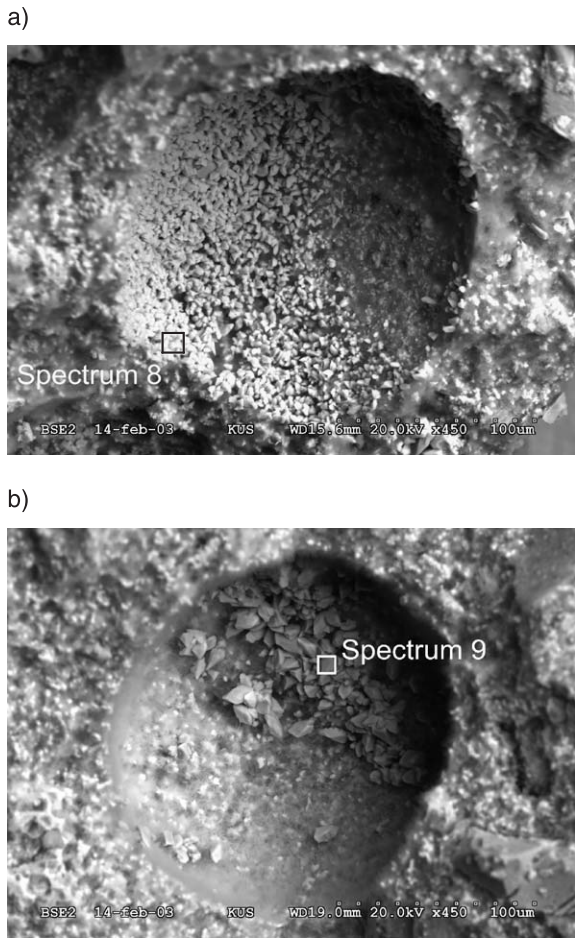

Fig. 6. SEM micrographs showing precipitation of calcite particles in the air voids after exposure (magnification: × 450). (a) 36 months naturally weathered; (b) 2500 h artificially weathered.

Table 3
EDS data of Spectrum 8 in Fig. 6a

Element	Weight (%)	Atomic (%)
C	2.4	4.1
O	59.1	75.8
Al	0.3	0.2
Si	1.8	1.3
S	0.2	0.2
Ca	35.8	18.3
Fe	0.4	0.1
Total	100.0	100.0

alternate wetting and drying cycles giving the strongest degradation effects to the surface. Thus, the exposed surface is quite as porous as what was also illustrated in the thin-section images. After longer exposure periods, either naturally or artificially, the calcite layer formations were washed out because of the Ca leachate, which was also indicated by the EDS analyses mostly exhibiting strong Si and O peaks.

Fig. 8 shows gypsum crystal growth forming a layer on the air-void wall after artificial exposure. This type of gypsum crystallisation was only observed in the artificially exposed samples, probably as a result of reaction of anhydrite with water to gypsum. Beneath the gypsum layer, small calcite particles were observed as well all over the solid matrix. While the concentration of calcite crystals changed as a function of depth from the exposed surface and was decreasing inwards, the gypsum crystals concentrated locally and occurred randomly at some distance from the artificially exposed surface. The dissolved gypsum crystals of the surface layer probably migrated to the inner parts due to changing moisture and temperature conditions. The needle-shaped single gypsum crystals were first gathered and eventually converted into thin-layer formations in a pattern. The forces exerted during crystallisation possibly caused gypsum growth to occur in the free air-void spaces, covering usually the larger air-void walls. On the other hand, the naturally weathered samples exhibited almost no gypsum recrystallisation subsurface; however, extensive gypsum crystalline deposits were observed on the exposed surface. Table 6 shows the corresponding EDS data from the selected target in Fig. 8.

Table 4
EDS data of Spectrum 9 in Fig. 6b

Element	Weight (%)	Atomic (%)
O	36.3	58.0
Mg	0.2	0.2
Al	0.6	0.6
Si	4.4	4.0
K	0.2	0.1
Ca	58.3	37.1
Total	100.0	100.0

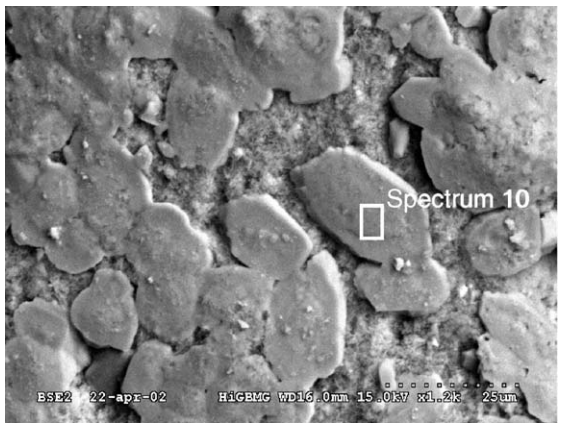

Fig. 7. SEM micrograph showing layer formation of calcite crystals on the 1500-h artificially weathered AAC surface (magnification: × 1.2k).

Gypsum crystal growth pattern on the exposed surface after natural weathering is shown in Fig. 9. The unexposed samples generally showed evenly distributed gypsum single crystals in the AAC, while recrystallised and gathered needle-shaped gypsum were mostly found in the aged samples. Growth of gypsum crystals on the surface of aged AAC was mostly found on the naturally exposed samples. Similar patterns were also detected on the 500- and 1500-h artificially aged sample surfaces, but these occurred seldom and the scope was much smaller than seen on the naturally weathered samples. EDS analysis of naturally weathered surfaces also indicated that the sulphur concentration was much more dominating compared to that of the artificially exposed surfaces. This may partly be related to the externally penetrated sulphate ions originating from the atmospheric pollution and partly to the fact that, contrary to the gypsum in the artificially weathered samples, the gypsum in the original material moved towards the surface layer and concentrated there. Besides, the pattern slightly differs from those formed in the air voids inside the artificially aged material (Fig. 8). This flowerlike surface gypsum pattern is probably what usually is called efflorescence formation after weathering. After longer exposure, this gypsum growth pattern even turned into a more diffused form and lost its (flowerlike) thin vein shape. The EDS spectrum (Table 7)

Table 5
EDS data of Spectrum 10 in Fig. 7

Element	Weight (%)	Atomic (%)
C	3.2	5.8
O	49.6	67.6
Mg	0.6	0.5
Al	0.2	0.2
Si	2.2	1.7
S	1.2	0.8
K	0.2	0.1
Ca	42.9	23.3
Total	100.0	100.0

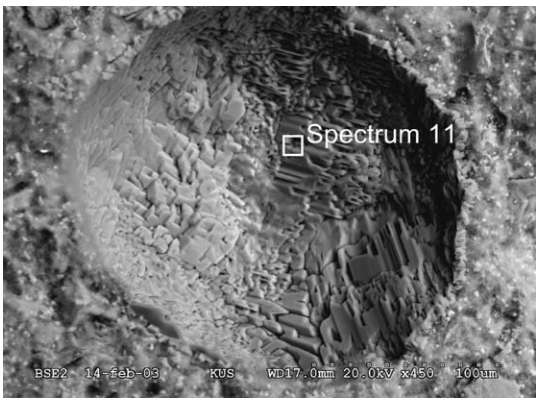

Fig. 8. SEM micrograph showing gypsum recrystallisation in the 2500-h artificially weathered AAC sample gradually covering the air-void walls after exposure (magnification: × 450).

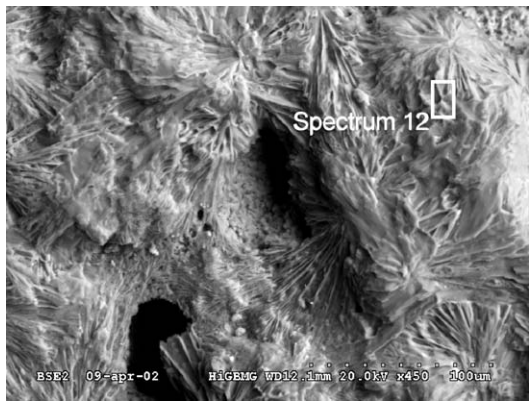

Fig. 9. SEM micrograph showing gypsum crystal growth pattern on the 6-m naturally weathered AAC surface after exposure (magnification: × 450).

exhibited high S, O and C peaks with minimal reading of Si. The high sulphur content indicates that the crystal growth is possibly gypsum ($CaSO_4$).

3.3. X-ray diffraction

The specific peaks in the XRD analysis corresponding to the binder of AAC mainly indicate the presence of tobermorite and calcite as might be expected. Figs. 10 and 11 show the diffraction patterns of the naturally and artificially weathered samples, respectively. The peaks of calcite, for the weathered samples, and the peaks of anhydrite and tobermorite, for the unexposed samples, all exhibited rather strong intensity. Gypsum peaks can also be identified, but not so clearly as gypsum visually indicated in the SEM micrographs.

The XRD pattern of the unexposed sample was measured after 4 years of storage in the laboratory. Accordingly, the reference-unexposed sample demonstrated some amount of calcite, in spite of the fact that it was not directly exposed. This agrees with the SEM results, which also confirm the presence of small particles of calcite in the unexposed sample, actually not being a fresh material, as mentioned before. The tobermorite content of this sample was slightly lower as compared to that of entirely fresh material, which was examined directly after being produced (not reported here). In general, the contents of tobermorite (T) and anhydrite (A) decreased while calcium carbonate in the form of calcite (C) significantly increased with exposure time. The anhydrite was probably converted into the more stable form of calcium sulphate, gypsum. Although the SEM + EDS examinations clearly demonstrated the presence of gypsum crystals, gypsum in the aged samples could not be uniquely identified by XRD, except for the 36-month naturally exposed sample, which exhibited somewhat stronger peaks. The formation of gypsum on the 36-month naturally exposed sample surfaces may also be due to atmospheric sulphur. Also SEM + EDS surface analysis verifies this, revealing a rather high sulphur concentration with sulphur covering the entire surface of the naturally exposed samples.

As can be seen in the figures, the samples exposed naturally and artificially exhibited similar results regarding carbonation. However, after 36 months of natural exposure, the tobermorite content of AAC decreased relatively more when compared to that of the 2500-h artificially exposed ones. Consequently, the content of calcite for the 36-month naturally exposed AAC is relatively higher than that of the 2500-h artificially exposed ones.

The reason why gypsum was not clearly detected by XRD may have several explanations. Firstly, the overall amount of gypsum in the AAC material is normally small, and therefore the intensity of the gypsum peaks is weak in the XRD pattern. SEM micrographs demonstrate also that in the aged samples, particularly during artificial weathering, gypsum recrystallised and formed very thin layers covering

Table 6
EDS data of Spectrum 11 in Fig. 8

Element	Weight (%)	Atomic (%)
O	66.3	81.5
Si	1.0	0.7
S	14.4	8.8
Ca	18.3	9.0
Total	100.0	100.0

Table 7
EDS data of Spectrum 12 in Fig. 9

Element	Weight (%)	Atomic (%)
O	58.9	76.1
Mg	0.1	0.1
Al	0.4	0.3
Si	4.0	3.0
S	13.5	8.7
Ca	22.8	11.7
Fe	0.3	0.1
Total	100.0	100.0

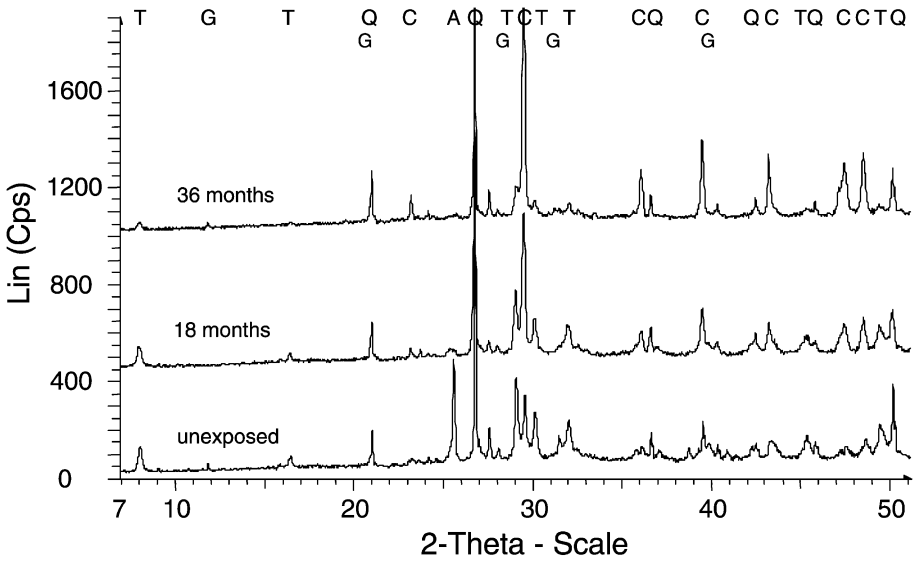

Fig. 10. XRD patterns of naturally weathered AAC [tobermorite (T), quartz (Q), calcite (C), anhydrite (A) and gypsum (G)].

some of the air-void walls and occurred mostly as local concentrations at some distance from the exposed surface. Since the powdered samples of the XRD analysis were taken from the surface layer, the recrystallised gypsum in the artificially weathered samples was possibly not included in these analysed amounts. The progressive propagation of carbonation in the aged samples, on the contrary, led to a high amount of calcite crystals homogeneously precipitated all over the surface zone. Thus, the calcite peaks in the XRD increased significantly, in proportion to phase concentration increasing with time. Secondly, some of the gypsum peaks overlapped the peaks of quartz, calcite and tobermorite. Thirdly, XRD is not sensitive enough to clearly detect the gypsum mineral phase in the AAC. Nevertheless, the presence of gypsum is also confirmed by the XRD results, at least for the unexposed and the 36-month naturally weathered samples.

4. Conclusions

In order to better understand the long-term performance and durability of porous building materials, the microstructural characteristics of naturally and artificially aged AAC samples, as well as unexposed ones, were investigated. Different phase formations during exposure were observed by means of thin-section and electron microscopy, and the results were supported by chemical and structural analysis using XRD and EDS. One of the important degradation mechanisms caused by water is the propagational dissolu-

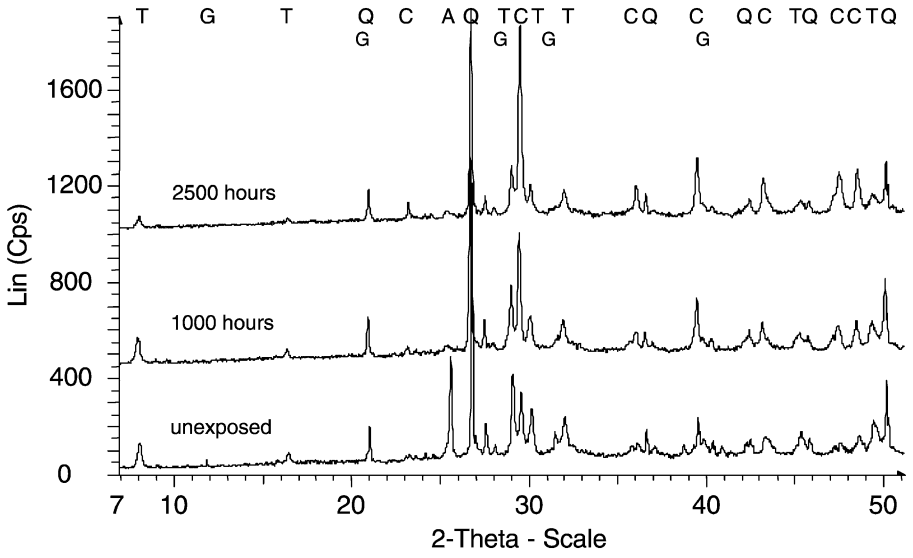

Fig. 11. XRD patterns of artificially weathered AAC [tobermorite (T), quartz (Q), calcite (C), anhydrite (A) and gypsum (G)].

tion of binding agents such as C-S-H, for AAC mostly in the form of tobermorite, particularly at the surface zone. A gradual leaching out with time from the surface of aged AAC samples was visually confirmed by thin-section images. CO_2, either dissolved in water or as gas, attacks tobermorite, portlandite and other C-S-H gels forming $CaCO_3$, which is known as carbonation. XRD patterns demonstrated decreased concentration of tobermorite but increased concentration of calcite with exposure time. Gradual growth of calcite crystals during exposure was clearly detected in the SEM examinations in the form of widespread precipitation in the air voids as well as in the solid matrix. Another type of crystal growth observed on the air-void walls and on the surface of AAC was gypsum. Layer formations in or filling up the air voids by crystal growth change the void size distribution in the material, which is strongly decisive for its frost resistance. On the other hand, moisture transport, i.e., wetting and drying properties, is also influenced, which in turn may lead to a faster degradation. Similarities were found in both naturally and artificially weathered samples as for the aforementioned mechanisms. However, samples exposed to real atmospheric conditions were further experienced, among other pollutants, atmospheric gaseous SO_2, leading to gypsum development and subsequent Ca leaching, which resulted in relatively higher erosion of surfaces than those of the artificially weathered ones.

The overall results indicate that after longer periods of exposure, the naturally weathered AAC surface differs somewhat in microstructural characteristics from that of the artificially weathered sample surfaces. The 36-month naturally exposed samples generally exhibited a rough and spongy surface character in addition to accumulated dirt in the visual SEM examinations, and the EDS data demonstrated higher sulphur content for the surface layer, probably contaminated via dry and wet deposition. On the other hand, the artificially exposed sample surfaces were not deteriorated that much, at least in the similar way. The alteration features observed on the naturally exposed surfaces are probably because of the deteriorating effects of air contaminants, particularly SO_2, which were not included in the artificial exposure test. The long-term effect of natural weathering is also confirmed by the test results of the physical properties such as water absorption and drying out [11]. The deteriorating effects of air contaminants on AAC are very complex since many variables are involved and need to be clarified by further research with complementary-analysed techniques.

Biological growth is another type of degradation mechanism, some evidence of which was found at SEM examinations, particularly for the naturally exposed AAC. However, this subject will be separately studied using appropriate methods for identification of microorganisms and their effects.

Prediction of service life and durability can only be made by characterisation of both the material properties and the microenvironment. As for other wall types, protection of AAC against outdoor conditions, particularly rain, plays an important role for the service life. Therefore, different coatings and external rendering systems are applied to improve resistance to environmental factors. Research on the microenvironmental characterisation of rendered AAC walls is still going on [12].

Since the performance of inorganic materials is mainly governed by its mineralogical composition, microscopic and spectrographic analyses are found to be of high importance. After determination and description of degradation mechanisms on the microstructural level, further work will include the completion of the experimental studies with quantification and modelling in terms of dose–response functions, which may be used in long-term performance estimations of AAC.

References

[1] S. Aroni, G.J. de Groot, M.J. Robinson, G. Svanholm, F.H. Wittman (Eds.), Autoclaved Aerated Concrete: Properties, Testing and Design, RILEM Recommended Practice, E&FN Spon, London, 1993.
[2] F. Matsushita, Y. Aono, S. Shibata, T. Kamada, Microstructure of autoclaved aerated concrete subjected to carbonation, Proceedings of 8th International Conference on Durability of Building Materials and Components (8DBMC), Vancouver, 1999, June, pp. 159–169.
[3] F. Matsushita, Y. Aono, S. Shibata, Carbonation degree of autoclaved aerated concrete, Cem. Concr. Res. 30 (2000) 1741–1745.
[4] H. Kus, Moisture performance evaluation of rendered autoclaved aerated concrete by microstructure characterisation, Proceedings of the 8th Euroseminar on Microscopy Applied to Building Materials, Athens, 2001, September 4–7, pp. 183–190.
[5] G. Fortunati, A. Dal Bo, I. Torresan, G. Biscontin, G. Driussi, Dehumidifying render for historic masonry: study of macro-porous mechanism and salt crystallisation inside pores, Proceedings of the 8th Euroseminar on Microscopy Applied to Building Materials, Athens, 2001, September 4–7, pp. 435–439.
[6] A.B. Leslie, J.J. Hughes, Complex structure and mineralogy of historic Scottish mortars—Implications for replacement mixes and repair strategies, Proceedings of the 8th Euroseminar on Microscopy Applied to Building Materials, Athens, 2001, September 4–7, pp. 443–450.
[7] D. Bajare, I. Rozenshrauha, L. Berzina, K. Sefarth, Changes in the microstructure during weathering and by using different additives, Proceedings of the 8th Euroseminar on Microscopy Applied to Building Materials, Athens, 2001, September 4–7, pp. 413–417.
[8] D. Hoffmann, K. Niesel, Quantifying the effect of air pollutants on renderings and also moisture-transport phenomena in masonry including its constituents, available at: http://www.bam.de/a_vii/moisture/transport.html (accessed June 15, 2002).
[9] A.E. Charola, Salts in the deterioration of porous materials: an overview, JAIC 39 (3) (2000) 327–343.
[10] ASTM G155-00a$^{\varepsilon 1}$, Standard Practice for Operating Xenon-Arc Light Apparatus for Exposure of Non-Metallic Materials, ASTM, PA, USA, 2001.
[11] H. Kus, Long-term performance of water repellants on rendered autoclaved aerated concrete, KTH-BMG, PhD Thesis, Gävle, 2002.
[12] H. Kus, K. Nygren, Microenvironmental characterization of rendered autoclaved aerated concrete, Build. Res. Int. 30 (1) (2002) 25–34.